Immunolocalization of skeletal matrix proteins in tissue and mineral of the coral *Stylophora pistillata*

Tali Mass[a], Jeana L. Drake[a], Esther C. Peters[b], Wenge Jiang[c], and Paul G. Falkowski[a,d,1]

[a]Environmental Biophysics and Molecular Ecology Laboratory, Institute of Marine and Coastal Sciences, Rutgers University, New Brunswick, NJ 08901; [b]Department of Environmental Science and Policy, George Mason University, Fairfax, VA 22030; [c]Faculty of Dentistry, McGill University, Montreal, QC, Canada H3A 0C7; and [d]Department of Earth and Planetary Sciences, Rutgers University, Piscataway, NJ 08854

Edited by Nancy Knowlton, Smithsonian Institution, Washington, DC, and approved July 24, 2014 (received for review May 9, 2014)

The precipitation and assembly of calcium carbonate skeletons by stony corals is a precisely controlled process regulated by the secretion of an ECM. Recently, it has been reported that the proteome of the skeletal organic matrix (SOM) contains a group of coral acid-rich proteins as well as an assemblage of adhesion and structural proteins, which together, create a framework for the precipitation of aragonite. To date, we are aware of no report that has investigated the localization of individual SOM proteins in the skeleton. In particular, no data are available on the ultrastructural mapping of these proteins in the calcification site or the skeleton. This information is crucial to assessing the role of these proteins in biomineralization. Immunological techniques represent a valuable approach to localize a single component within a calcified skeleton. By using immunogold labeling and immunohistochemical assays, here we show the spatial arrangement of key matrix proteins in tissue and skeleton of the common zooxanthellate coral, *Stylophora pistillata*. To our knowledge, our results reveal for the first time that, at the nanoscale, skeletal proteins are embedded within the aragonite crystals in a highly ordered arrangement consistent with a diel calcification pattern. In the tissue, these proteins are not restricted to the calcifying epithelium, suggesting that they also play other roles in the coral's metabolic pathways.

actin | carbonic anhydrase | CARPs | cadherins

Corals (phylum Cnidaria) belong to one of the oldest invertebrate phyla and are one of the earliest metazoans to possess an organized body structure (reviewed in ref. 1). The radial body plan of cnidarians consists of only two cell layers: an ectoderm and an endoderm, connected by the mesoglea, an extracellular gelatinous matrix containing collagen fibers and cells (2). In zooxanthellate corals, which arose in the early Mesozoic (3), the gastrodermis, which is derived from the endoderm, contains intracellular photosynthetic dinoflagellates of the genus *Symbiodinium* (commonly named zooxanthellae). The aboral ectoderm, which is mechanically anchored to the skeleton by desmocytes (4) and referred to as the calicoblastic epithelium (5) or calicodermis (6), appears to control the extracellular precipitation of aragonite fibrils (orthorhombic $CaCO_3$) (4, 7).

The resulting microscopic fibrils develop into a skeletal framework containing proteins and their glycosylated derivatives, commonly named skeletal organic matrix (SOM), with structural features that are genetically determined (8). However, although various aspects of biomineralization in corals have been studied for decades, the basic mechanism responsible for the precipitation of the aragonite skeleton remains enigmatic (reviewed in ref. 9).

All metazoan calcium carbonate biomineralization processes share a remarkable property: their skeleton formation is finely regulated by SOM, which remains embedded within the exoskeleton (10). The SOM (0.1–5 wt% of the skeleton) is composed of a mixture of macromolecules, mainly proteins, polysaccharides, and glycoproteins, which are secreted by the calcifying tissue during skeletogenesis and are associated with a 3D framework inside skeletal structures (11, 12). Understanding the spatial relationship between the organic and the mineral phases can help elucidate the functions of matrix components during crystal synthesis (13). During the past two decades, it has been shown that the basic skeletal units, crystal-like fibers, are built by repeated micrometer growth steps that can be visualized by etching polished skeletal surfaces (14–16). The resulting macroscopic skeletal structures of individual corals are strongly influenced by environmental factors, especially light (17), physical flow (18), and carbonate saturation (19). The aggregate of these individual coral skeletons is the basis for reef formation in tropical and subtropical shallow ocean margins, and is critical for the sustaining the diversity of fauna found in those environments (20).

X-ray absorption near edge structure spectroscopy mapping, at the micrometer scale, has established that the SOM is associated with the mineral phase within each growth layer (21). Recently, it was suggested that each couplet of organic-seed (e.g., negative etching) and fiber interaction represents a single 24-h period (22). However, despite numerous biochemical and structural studies, the precise localization of distinct SOM proteins and how these proteins interact with the mineral remains poorly understood.

In corals, the production of organic material is thought to be a prerequisite for calcification (23), with protein synthesis closely associated with calicodermal cells (24–26). The first published proteome analysis of the SOM in a stony coral (27) revealed a group of coral acid-rich proteins (CARPs) that can spontaneously catalyze the precipitation of calcium carbonate in vitro (28). The proteome also contained an assemblage of adhesion and structural proteins, which potentially create a framework for the precipitation of aragonite (27). Nevertheless, to date, carbonic anhydrase (CA; i.e, STPCA2) is the only SOM protein that has been localized in

Significance

Although various aspects of biomineralization in corals have been studied for decades, the basic mechanism responsible for the precipitation of the aragonite skeleton remains enigmatic. To address this issue, we used antibodies against key biomineralization proteins derived from the common zooxanthellate coral *Stylophora pistillata* to elucidate the spatial arrangement of specific skeletal matrix proteins in the skeleton and in the animal tissue. To our knowledge, our results reveal for the first time that the biomineral is produced in discrete nanoscale packages in which the secreted organic matrices remain entrapped within the crystalline units whose growth they control, leading to the formation of highly ordered, microscopic, heterologous structures, which are aggregated to form a macroscopic skeleton.

Author contributions: T.M. and P.G.F. designed research; T.M., J.L.D., and W.J. performed research; T.M., J.L.D., E.C.P., W.J., and P.G.F. analyzed data; and T.M., J.L.D., E.C.P., and P.G.F. wrote the paper.

The authors declare no conflict of interest.

This article is a PNAS Direct Submission.

[1]To whom correspondence should be addressed. Email: falko@marine.rutgers.edu.

This article contains supporting information online at www.pnas.org/lookup/suppl/doi:10.1073/pnas.1408621111/-/DCSupplemental.

www.pnas.org/cgi/doi/10.1073/pnas.1408621111

Downloaded at Palestinian Territory, occupied on December 9, 2021

www.manaraa.com

tissue; however, it was observed mainly in the oral and aboral gastrodermis and aboral calicodermis, and has not been immunolocated to any region of the skeleton (29). Moreover, no report has investigated the localization of any individual SOM proteins in the skeleton. In particular, no data are available on the ultrastructural mapping of these proteins in the calcification site or the skeleton. This information is crucial to assess the role of these proteins in biomineralization.

To address this key issue, we generated polyclonal antibodies to peptides derived from unique sequences of each of four CARPs and cadherin genes derived from the common zooxanthellate coral *Stylophora pistillata*. With these antibodies and those raised against an actin and a CA, we show here the spatial arrangement of key skeletal matrix proteins in the skeletal fibers and in the animal tissue by using immunohistochemistry (IHC) and immunogold labeling assays. By using high-resolution electron and atomic force microscopy (AFM), our results reveal that skeletal proteins are embedded within the aragonite crystal with unique, fan-like arrangements with ∼3-μm radii, consistent with a diel calcification pattern. Moreover, the spatial distribution of these proteins in the tissue and skeleton imply a temporal sequence of events throughout the biomineralization reaction in vivo.

Results

IHC. Thin sections of coral tissue from *Stylophora pistillata* were labeled with anti-CARPs 1–4, cadherin, actin, and CA (Fig. 1). All antibodies bound to the cells surrounding the skeleton in the calicodermis in addition to locations specific to each of the proteins as described later (Fig. 1). CARP 1 appears to be located in the oral epidermis in an area with direct contact to the seawater and in association with the nematocytes in the tentacles. CARPs 2 and 3 are located at the base of the nematocytes in the tentacles as well. CARP 4 is located in the oral epidermis and is the only protein that is also localized in desmocytes, which attach the tissue to the skeleton (4). The cadherin appears to be expressed at the base of the polyp cnidocyte batteries, an area rich with neurons (2, 30), whereas, in the epidermis, it is located only at cell membranes of cnidocytes. Cadherin, CA, and actin also appear to be located in the *Symbiodinium* sp. cells. Actin and CA are located in all epithelia but are not associated with areas that require high Ca^{2+} concentrations (i.e., cnidocytes and neurons). Almost no staining was observed in the negative control treatment performed without primary antibody.

Skeleton Growth Mode. Scanning EM imaging of gently etched, polished surfaces in the back-scattered electron mode reveals the common growth pattern of coral skeleton; this pattern results from differences in mineral solubility (Fig. 2 *A* and *B*) (15). This pattern shows the early mineralization zone (EMZ) and a repetitive, highly organized, concentric fiber growth step (FGS) of the crystals. The unit structure (Fig. 2*B*) is made of individual fibers ranging from 1 to 4 μm in length. AFM in the tapping mode revealed that the growth increments are actually submicron-sized skeletal fibers (Fig. 2 *C* and *E*) composed of densely packed nanograins surrounded by a cortex of an organic matrix phase (Fig. 2 *D* and *F*). AFM images confirm that fibers are not homogenous structures at the submicron scale. The high phase contrast supports the hypothesis that there is an organic coating of the inorganic nanoparticles, and suggests that coated nanoparticles are the minimum unit of organization of the fiber growth layers.

Immunogold Staining. Although the exact composition of the fiber growth layers and EMZ detailed earlier remains unknown, the results we present here suggest a distinct distribution of seven

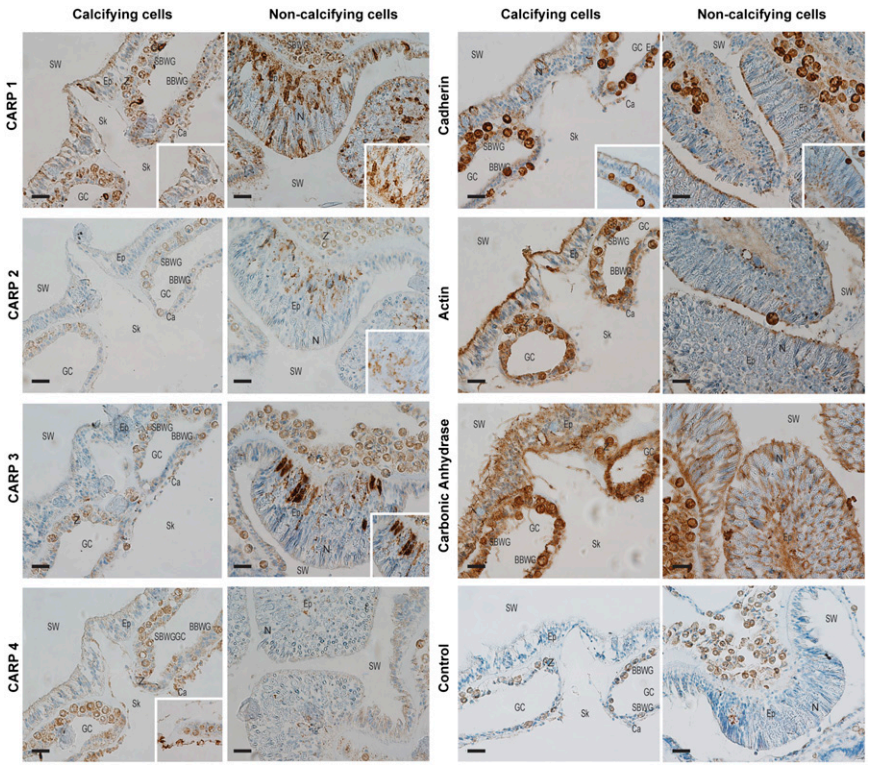

Fig. 1. Immunolabeling of tissues from *S. pistillata* embedded in paraffin. Tissue sections contain calcifying and noncalcifying cells as indicated by the headings. IHC of seven distinct SOM proteins reveals labeling at distinct intracellular localizations for each protein (brown), counterstained with hematoxylin (blue). (*Insets*) Specific localization of individual antibody labeling (magnification of 100×). BBWG, basal body wall gastrodermis; Ca, calicodermis; Ep, epidermis; GC, gastrovascular canal; N, nematocyte; SBWG, surface body wall gastrodermis; Sk, skeleton side; SW, seawater side; Z, zooxanthellae. (Scale bars: 20 μm.)

Downloaded at Palestinian Territory, occupied on December 9, 2021
www.manaraa.com

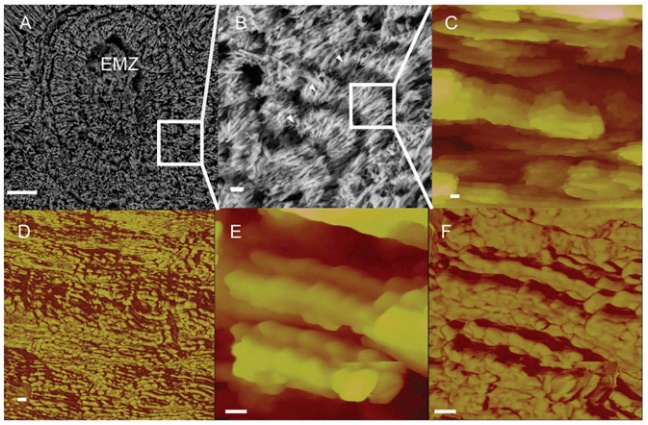

Fig. 2. Scanning EM images reveal the EMZ and FGSs (white arrowheads) in the *S. pistillata* skeleton (*A* and *B*). AFM of the reticulate structure of the skeleton at increasing magnification reveals the nanoscale building blocks (height images, *C* and *E*) and dual composition (phase images, *D* and *F*) of skeletal grains. Skeleton growth layers are composed of submicron-sized particles (*C* and *E*), which are a composite of an inorganic phase tens of nanometers in diameter (likely aragonite; yellow area in *D* and *F*) and an organic matrix phase (red area in *D* and *F*). (Scale bars: *A*, 10 μm; *B*, 1 μm; *C*–*F*, 100 nm.)

SOM proteins by immunogold labeling assays. Fig. 3 indicates that CARPs 1 and 4 are localized adjacent to the EMZ, whereas CARP 2 is associated with the more soluble region of the growth layer, and CARPs 3 and 4 and the cadherin are localized near the less soluble growth layers (Fig. 3). CA and actin show a similar distribution throughout the skeletal fibers. At higher magnification, it appears that the individual proteins are embedded in the mineral phase of individual fibers, which supports our AFM observations of mineral nanoparticles surrounded by an organic matrix containing at least CARPS 1–4 and the cadherin, CA, and actin described here (Fig. 3, *Insets*). Conversely, almost no particles were observed in the negative control treatments performed without primary antibody.

Discussion

To our knowledge, the results of this study reveal for the first time the spatial distribution of distinct SOM proteins in coral tissue and skeleton. The stony coral SOM contained CARPs that can spontaneously catalyze the precipitation of calcium carbonate in vitro (28) and an assemblage of adhesion and structural proteins, which potentially create a framework for the precipitation of aragonite (27).

It has been demonstrated previously by immunolabeling that the SOM protein complex and the bone morphogenetic protein (BMP2/4) are present only in calicodermal cells (23, 31), whereas the *S. pistillata* CA, STPCA-2, has been localized to the cytoplasm in the oral and aboral gastrodermis and the aboral calicodermis (29). It was proposed that the latter is involved in pH regulation and/or inorganic carbon delivery to symbiont and calcification (29). However, STPCA-2 homologs were detected in SOM by liquid chromatography/tandem MS (27, 32).

Further, we determined, by immunolocalization, the dispersal pattern of the seven SOM proteins in the animal and skeleton. These proteins are embedded within the aragonite crystals with unique arrangements and a highly controlled calcification pattern at the nanometer scale. However, in the tissue, these proteins are not restricted to the calcifying epithelium as was suggested previously (23), and instead often exhibit specific localization within noncalicodermal cells. With respect to the skeleton, the present study has much higher spatial resolution than previous studies (23), and confirms our proteomic analysis of *S. pistillata* SOM (27, 33). Hence, we are confident that localization of these proteins to noncalcifying cells represents cellular trafficking or multiple uses for each protein rather than contamination or nonspecific binding.

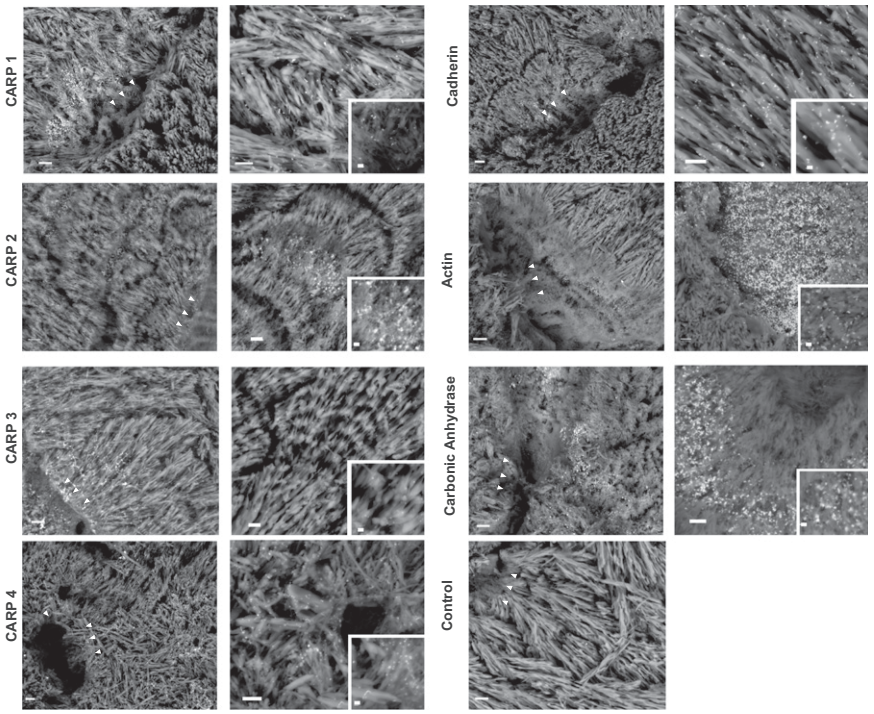

Fig. 3. Immunogold labeling of seven proteins on thin sections of skeletons from *S. pistillata*. The location of the individual proteins was observed by scanning EM in back-scattered electron mode. White arrowheads indicate the EMZ. (Scale bars: *Left*, 2 μm; *Right*, 1 μm; *Inset*, 0.2 μm.)

Downloaded at Palestinian Territory, occupied on December 9, 2021
www.manaraa.com

All seven proteins exhibit distinct intracellular localizations in the tissue. CARPs 1–3 are highly expressed in two very different places, one being the calcifying tissue and the second in the base of nematocytes (i.e., stinging cells), an area with high calcium concentration (34). Furthermore, the latter area is also rich in rough endoplasmic reticulum (ER). It has been reported that the majority of intracellular Ca^{2+} is bound to calcium-binding proteins and sequestered in the rough ER (35). CARPs 2 and 3 contain an isoleucine-proline-valine–like motif following the signal peptide sequence that has previously been suggested to assist in the trafficking of secreted, acidic, calcium-binding proteins out of the rough ER in metazoans (36). This suggests that these matrix proteins likely follow the classical routes of secretory protein assembly and export in eukaryotes, similar to what has been found in sea urchins (37, 38). The proteins are modified in the ER, exported in Golgi vesicles to the calicodermal layer, and eventually secreted into calcification sites. Nevertheless, in the skeleton, it appears that CARPs 2 and 3 are abundant in regions of more and less etching sensitivity, respectively. Intriguingly, CARP1 has the C-terminal HDEL and the initial acidic amino acid, EGD, motifs. These two are typical ER retention motifs (reviewed in refs. 39, 40). Despite these motifs, it has been shown that some calcium-binding ER resident proteins can be released from cells (41, 42). Additionally, calcium depletion may disrupt the conformation of the HDEL domain to reduce the effectiveness of the retention mechanism (43). In the skeleton, CARP 1 localizes around centers of calcification or EMZs, which, as a result of variable solubility of the biomineral at the nanoscale (15), are revealed by the etching process. The fact that CARP 4 is present in the desmocytes and the skeleton supports the hypothesis that desmocytes become interred in the skeleton as mineral is precipitated and are thereafter replaced by new desmocytes (4). The distribution of CARPs in the tissue is consistent with the previously described pattern of calcium distribution across the cell layers (34, 44).

The role of cadherin and actin in strengthening the integrity of the dorsal side of epithelium cells is well-established (45), which explains the presence of these two proteins at the apical regions of adjacent oral epidermal cells. Actin, a common cytoskeletal protein with high sequence conservation across the tree of life, including in *Symbiodinium* spp., has been shown to be important for coral organic matrix synthesis and calcification (46) and was observed in our study in endo- and ectodermal cells as well as the symbiont. Cadherin can be seen at polyp cnidocyte batteries in addition to the calicodermis and the skeleton. This is not surprising, as the polyp battery is an area rich with neurons (2, 30), and it has been suggested that the cadherin superfamily regulates the contacts or signaling between neurons in a variety of ways (47). Like actin, cadherin is observed in endo- and ectodermal cells and in the symbiont. However, neither the DNA sequence (GenBank accession no. AG3636.1) nor the peptide sequence against which the anti-cadherin antibody was raised (DYETKPTYTIKVTATDRK) produced blast hits against the *Symbiodinium minutum* nuclear genome (48). Hence, it is possible that the antibody is exhibiting nonspecific binding to an unknown *Symbiodinium* sp. protein. Additionally, cadherin is observed in all calicodermal cell membranes, and not specifically desmocytes, as well as throughout the etched skeleton regardless of the crystal patterns. Unlike cadherin, however, actin exhibits specific patterning in the skeleton, with higher abundance in regions more sensitive to etching.

CA was detected in membranes of all cell types including *Symbiodinium* spp., as well as intracellularly in host calicodermis and symbiont cells. CA is integral to intracellular pH homeostasis (host and symbiont) (49) and a source of CO_2 to the RuBisCo enzyme for carbon fixation (symbiont) (50). The CA antibody we used is not specific to the STPCA2 protein found intracellularly in calicodermal cells (29) or in coral skeleton (27, 32). Therefore, it may bind to a variety of CAs produced by host and symbiont and may explain its wide distribution throughout tissue in this study. However, STPCA2 is the only CA to date that has been sequenced from the skeleton (27, 32). Additionally, as we show, the antibody binds a glycosylated protein of ∼40 kDa in organic matrix extracted from *S. pistillata* skeleton and, therefore, it is likely that the antibody is binding STPCA2 ubiquitously in the etched skeleton (Fig. S1).

By etching the polished surface of thin sections of newly cleaned coral skeletons, scanning EM imaging reveals the fiber growth layers that accumulate in the skeleton along successive growth steps with alternating bands of sensitivity to dissolution (Fig. 3 *A* and *B*) (15). Each layer is ∼2 to 5 μm thick, which likely represents a single day's growth (22, 51). The thickening of the septa is ensured by superimposition of growth layers that surround the EMZ (14, 15, 52). It has been suggested that more than one growth layer is formed each day (15). AFM in the tapping mode reveals that coral fibers are not homogenous structures at the submicron scale, but are instead made of nanoparticles densely packed within an organic matrix (Fig. 3 *C* and *E*). In addition, immunolabeling has shown that the anti-total SOM serum reacts with two different skeleton structures, the corallite and the coenosteum (23), although the relatively low magnification precluded the ability to visualize binding to individual fibers. However, these authors suggest that the organic matrix coats bundles of fibers rather than individual fibers. In the present study, by using high-resolution field emission scanning EM, a positive labeling by anti-CARP 1–4, a cadherin, an actin, and a CA (STPCA2; GenBank accession no. EU532164.1) of the skeletal fibers was observed. Hence, it appears that SOM proteins coat individual fibers as well as fiber bundles. In addition, the distribution of the labeling strongly suggests that organic components are intimately associated with the mineral phase, and the skeletal proteins are actually embedded within aragonite crystal-like fibers (Fig. 3) with a unique role to each protein. AFM images in high phase contrast reveal that each growth layer represents the superimposed succession of several repeated organic seed–fiber interactions (Fig. 3 *D* and *F*).

Based on these results, we propose a working model of the calcification mechanism (Fig. 4). The spatial distribution of these proteins in the tissue and skeleton implies specific roles for each protein and a temporal sequence of events throughout the biomineralization process in vivo. In the tissue, cadherin has a role in intercellular adhesion and attaching the cells to the skeleton. Additionally, actin is a component of cellular molecular motors (53). Attachment of cells to skeleton should occur during the day and night and would require a degree of flexibility in the molding of the calcifying space. Another stabilizing protein (CARP 4) anchors the desmocytes of the calicodermis to the skeleton. Hence, cadherin, actin, and CARP 4 are found throughout the skeleton regardless of day/night crystal patterns. Additionally, cadherin and CARP 4 were observed with a strong e-value in proteomic analyses of coral SOM (27, 32). Combined, this information suggests that cadherin and CARP4 are relatively highly abundant proteins in coral skeleton. CARPs 1–3 trap and direct Ca^{+2} to calcification sites with specific roles assigned to each protein. CARPs 1 and 4 form crystal binding substrates that lead to $CaCO_3$ nucleation, as evidenced by their presence in the EMZs, similar to osteopontin, which nucleates human kidney stones (54). CARP 2's role is in extension, potentially at night, contributing to the more soluble FGS. CARPs 3 and 4 infill the skeletal mold, potentially during the photoperiod, and contribute to less soluble growth layers, thus guiding the crystals to specific orientations. CA participates in pH homeostasis by compensating for the H^+ released as the CARPs induce Ca^{2+} into a Lewis acid reaction with soluble bicarbonate anions (28).

Overall, it is becoming increasingly clear that the model of "biologically controlled mineralization" (14, 55) in corals is very precisely regulated by a relatively small set of proteins at the

Downloaded at Palestinian Territory, occupied on December 9, 2021
www.manaraa.com

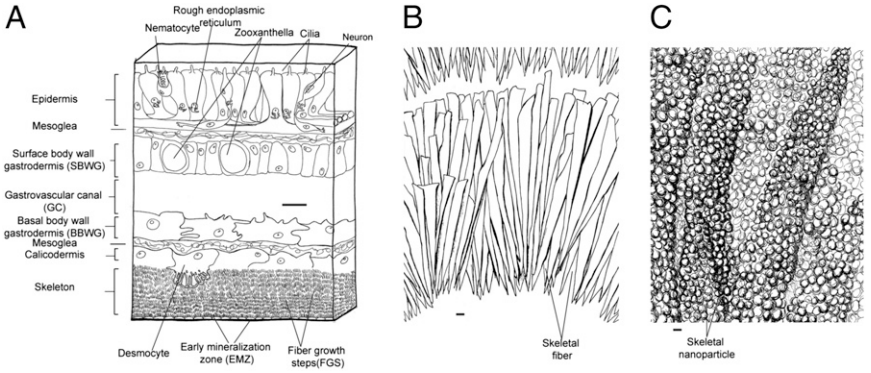

Fig. 4. Cross-sectional drawing of the histology of coral tissue and skeleton, suggesting a mechanistic understanding of the skeletal growth layers (*A*). The spatial distribution of SOM proteins are indicated and are suggested to be involved in a diel pattern of skeletal linear extension (night) and skeletal thickening (day) (*B*). The crystalline units are composed of submicron-sized particles coated with organic matter (*C*). (Scale bars: *A*, 10 μm; *B*, 1 μm; *C*, 100 nm.)

nanometer scale. A diel pattern of skeletal linear extension at night and skeletal thickening ("infilling") during the day were previously observed in symbiotic corals (e.g., refs. 51, 56–58). However, a recent study using secondary ion mass spectrometry shows that the two common microstructural components, centers of calcification and fibers, are produced during day and night (59). In addition, in asymbiotic deep-sea corals, EMZs and fibrous layers have been observed (21). Regardless of the timing, however, at each growth step, the secreted organic matrices remain entrapped within the crystalline units whose growth they control, leading to the formation of heterologous structures revealed by the etching process (16). Exactly how the specific proteins control the orientation of the nanocrystals clearly remains one of the most challenging aspects of biomineralization in the evolutionary development of corals and other biomineralizing organisms (60).

Materials and Methods

A complete description of the study methods is provided in *SI Materials and Methods*.

Sample Preparation for Immunolocalization. ***Polyclonal antibody production.*** Custom-made polyclonal antibodies were raised against the CARP proteins and a cadherin by Thermo Scientific Pierce Custom Antibody Services. We used these antibodies and those raised against human β-actin actin (PA5-16914; Pierce) and a CA (61) to analyze the spatial arrangement of the proteins. All of the *Stylophora*-specific antibodies used in this study showed a distinct immunoreactivity (28) (Fig. S1).

Immunohistochemical localization. *S. pistillata* nubbins were fixed in Z-fix (Anatech), slowly decalcified. and embedded in paraffin. All IHC was performed by using a Ventana Medical Systems Discovery XT automated immunostainer. Primary anti-CARPs 1–4, -cadherin, -actin, and -CA were applied at 1:800, 1:50, 1:200, 1:2,000, 1:500, 1:200, and 1:5,000 dilution, followed by application of prediluted universal secondary antibody (no. 760–4205; Ventana Medical Systems) and then a chromogenic detection kit (DABMap; no. 760–124; Ventana Medical Systems). Hematoxylin was used as a counterstain. Control experiments were performed similarly without the first antibody step, diluted as described earlier.

Immunogold localization. Thin sections of *S. pistillata* skeleton were embedded in Buehler C-D epoxy, ground and polished to a final thickness of ~30 μm, and mirror-polished before immunogold labeling. Thin sections were cleaned with dilute sodium hypochlorite, slightly etched with EDTA, and blocked with filtered gelatin in Tris-buffered saline (TBS) solution, pH 7.5. The sections were incubated with an antibody raised against CARPs1–4, cadherin, actin, or CA, diluted as follows: 1:1,000 (CARPs 1–2), 1:500 (CARPs 3–5, actin), 1:100 (cadherin), and 1:5,000 (CA) in 1% gelatin in TBS solution, pH 7.5, containing Tween 20 (0.05% vol/vol). Control sections were incubated without primary antibody (Fig. 3). After extensive rinsing, sections were incubated in a secondary antibody (goat anti-rabbit coupled to 18-nm gold particles; 111215144; Jackson ImmunoResearch) diluted 1:20 in 0.05% TBS–Tween solution, pH 7.5. Preparations were then dried before silver enhancement (Sigma). Sections were dried and carbon-sputtered for field emission scanning EM observations (Sigma; Zeiss).

AFM. AFM images were collected on a mirror-polished clean surface in tapping mode with a multimode scanning probe microscope by using a DI Nano IIIa instrument (Veeco). Phase images were generated by AFM cantilever frequency shift as the difference between organic matrix and inorganic aragonite compositions.

ACKNOWLEDGMENTS. We thank J. Yaiullo (Long Island Aquarium), L. Cong (histopathology and imaging services, Cancer Institute of New Jersey), M. K. Battles, L. Haramaty, L. Fisher, S. Murali, F. Natale, C. Vidito, K. Wyman, and V. Yamazaki, and F. Morel (Princeton University) for the gift of the custom-made CA antibody (GenBank accession no. AAX08632.1). This research was supported by National Science Foundation Grant EF1041143.

1. Erwin DH, et al. (2011) The Cambrian conundrum: Early divergence and later ecological success in the early history of animals. *Science* 334(6059):1091–1097.
2. Fautin DG, Mariscal RN (1991) Cnidaria: Anthozoa. *Microscopic Anatomy of Invertebrates: Placozoa, Porifera, Cnidaria, and Ctenophora*, eds Harrison FW, Westfall JA (Wiley-Liss, New York), Vol 2, pp 267–358.
3. Stanley GD (2003) The evolution of modern corals and their early history. *Earth Sci Rev* 60(3-4):195–225.
4. Muscatine L, Tambutte E, Allemand D (1997) Morphology of coral desmocytes, cells that anchor the calicoblastic epithelium to the skeleton. *Coral Reefs* 16(4):205–213.
5. Von Heider A (1881) Die gattung cladocora ehrenb. *Sber Akad Wiss Wien* 84:634–637.
6. Galloway SB, et al. (2007) *Coral Disease and Health Workshop: Coral Histopathology II. NOAA Technical Memorandum NOS NCCOS 56 and CRCP 4* (National Oceanic and Atmospheric Administration, Silver Spring, MD).
7. Tambutte E, et al. (2007) Observations of the tissue-skeleton interface in the scleractinian coral *Stylophora pistillata*. *Coral Reefs* 26(3):517–529.
8. Allemand D, Tambutté É, Zoccola D, Tambutté S (2011) Coral calcification, cells to reefs. *Coral Reefs: An Ecosystem in Transition*, eds Dubinsky Z, Stambler N (Springer, New York), pp 119–150.
9. Tambutté S, et al. (2011) Coral biomineralization: From the gene to the environment. *J Exp Mar Biol Ecol* 408(1–2):58–78.
10. Lowenstam HA, Weiner S (1989) *On Biomineralization* (Oxford Univ Press, Oxford).
11. Mann S (2001) *Biomineralization: Principles and Concepts in Bioinorganic Materials Chemistry* (Oxford Univ Press, New York).
12. Addadi L, Weiner S (1985) Interactions between acidic proteins and crystals: Stereochemical requirements in biomineralization. *Proc Natl Acad Sci USA* 82(12):4110–4114.
13. Weiner S, Addadi L (1997) Design strategies in mineralized biological materials. *J Mater Chem* 7(5):689–702.
14. Cuif J-P, Bendounan A, Dauphin Y, Nouet J, Sirotti F (2013) Synchrotron-based photoelectron spectroscopy provides evidence for a molecular bond between calcium and mineralizing organic phases in invertebrate calcareous skeletons. *Anal Bioanal Chem* 405(27):8739–8748.
15. Cuif JP, Dauphin Y (2005) The environment recording unit in coral skeletons - a synthesis of structural and chemical evidences for a biochemically driven, stepping-growth process in fibres. *Biogeosciences* 2(1):61–73.
16. Cuif JP, Dauphin Y, Freiwald A, Gautret P, Zibrowius H (1999) Biochemical markers of zooxanthellae symbiosis in soluble matrices of skeleton of 24 Scleractinia species. *Comp Biochem Physiol A Mol Integr Physiol* 123(3):269–278.
17. Einbinder S, et al. (2009) Changes in morphology and diet of the coral *Stylophora pistillata* along a depth gradient. *Mar Ecol Prog Ser* 381:167–174.

Downloaded at Palestinian Territory, occupied on December 9, 2021
www.manaraa.com

18. Mass T, Genin A (2008) Environmental versus intrinsic determination of colony symmetry in the coral *Pocillopora verrucosa*. *Mar Ecol Prog Ser* 369:131–137.
19. Cohen AL, McCorkle DC, de Putron S, Gaetani GA, Rose KA (2009) Morphological and compositional changes in the skeletons of new coral recruits reared in acidified seawater: Insights into the biomineralization response to ocean acidification. *Geochem Geophys Geosyst* 10:Q07005.
20. Dubinsky Z, Stambler N eds (2011) *Coral Reefs: An Ecosystem in Transition* (Springer, New York).
21. Cuif JP, Dauphin Y, Doucet J, Salome M, Susini J (2003) XANES mapping of organic sulfate in three scleractinian coral skeletons. *Geochim Cosmochim Acta* 67(1):75–83.
22. Wooldridge S (2013) A new conceptual model of coral biomineralisation: Hypoxia as the physiological driver of skeletal extension. *Biogeosciences* 10:2867–2884.
23. Puverel S, et al. (2005) Antibodies against the organic matrix in scleractinians: A new tool to study coral biomineralization. *Coral Reefs* 24(1):149–156.
24. Johnston IS (1980) The ultrastructure of skeletogensis in hermatypic corals. *Int Rev Cytol* 67:171–214.
25. Clode PL, Marshall AT (2003) Calcium associated with a fibrillar organic matrix in the scleractinian coral *Galaxea fascicularis*. *Protoplasma* 220(3-4):153–161.
26. Goldberg WM (2001) Acid polysaccharides in the skeletal matrix and calicoblastic epithelium of the stony coral *Mycetophyllia reesi*. *Tissue Cell* 33(4):376–387.
27. Drake JL, et al. (2013) Proteomic analysis of skeletal organic matrix from the stony coral *Stylophora pistillata*. *Proc Natl Acad Sci USA* 110(10):3788–3793.
28. Mass T, et al. (2013) Cloning and characterization of four novel coral acid-rich proteins that precipitate carbonates *in vitro*. *Curr Biol* 23(12):1126–1131.
29. Bertucci A, Tambutté S, Supuran CT, Allemand D, Zoccola D (2011) A new coral carbonic anhydrase in *Stylophora pistillata*. *Mar Biotechnol (NY)* 13(5):992–1002.
30. Peters EC, Anatomy. *Diseases of Corals*, eds Downs C, Woodley C, Porter J, Bruckner A (Blackwell, Oxford), in press.
31. Zoccola D, et al. (2009) Specific expression of BMP2/4 ortholog in biomineralizing tissues of corals and action on mouse BMP receptor. *Mar Biotechnol (NY)* 11(2): 260–269.
32. Ramos-Silva P, et al. (2013) The skeletal proteome of the coral *Acropora millepora*: The evolution of calcification by co-option and domain shuffling. *Mol Biol Evol* 30(9): 2099–2112.
33. Drake JL, et al. (2013) Reply to Ramos-Silva et al.: Regarding coral skeletal proteome. *Proc Natl Acad Sci USA* 110(24):E2147–E2148.
34. Marshall AT, Clode PL, Russell R, Prince K, Stern R (2007) Electron and ion microprobe analysis of calcium distribution and transport in coral tissues. *J Exp Biol* 210(pt 14): 2453–2463.
35. Pozzan T, Rizzuto R, Volpe P, Meldolesi J (1994) Molecular and cellular physiology of intracellular calcium stores. *Physiol Rev* 74(3):595–636.
36. von Marschall Z, Mok S, Phillips MD, McKnight DA, Fisher LW (2012) Rough endoplasmic reticulum trafficking errors by different classes of mutant dentin sialophosphoprotein (DSPP) cause dominant negative effects in both dentinogenesis imperfecta and dentin dysplasia by entrapping normal DSPP. *J Bone Miner Res* 27(6): 1309–1321.
37. Benson NC, Benson SC, Wilt F (1989) Immunogold detection of glycoprotein antigens in sea urchin embryos. *Am J Anat* 185(2-3):177–182.
38. Ameye L, Hermann R, Killian C, Wilt F, Dubois P (1999) Ultrastructural localization of proteins involved in sea urchin biomineralization. *J Histochem Cytochem* 47(9): 1189–1200.
39. Pelham HRB (1989) Control of protein exit from the endoplasmic reticulum. *Annu Rev Cell Biol* 5(1):1–23.
40. Pelham HRB (1990) The retention signal for soluble proteins of the endoplasmic reticulum. *Trends Biochem Sci* 15(12):483–486.
41. Maguire M, Coates ARM, Henderson B (2002) Chaperonin 60 unfolds its secrets of cellular communication. *Cell Stress Chaperones* 7(4):317–329.
42. Roberts MM, et al. (2003) *Mycobacterium tuberculosis* chaperonin 10 heptamers self-associate through their biologically active loops. *J Bacteriol* 185(14):4172–4185.
43. Jeffery E, Peters LR, Raghavan M (2011) The polypeptide binding conformation of calreticulin facilitates its cell-surface expression under conditions of endoplasmic reticulum stress. *J Biol Chem* 286(4):2402–2415.
44. Clode PL, Marshall AT (2004) Calcium localisation by X-ray microanalysis and fluorescence microscopy in larvae of zooxanthellate and azooxanthellate corals. *Tissue Cell* 36(6):379–390.
45. Baum B, Georgiou M (2011) Dynamics of adherens junctions in epithelial establishment, maintenance, and remodeling. *J Cell Biol* 192(6):907–917.
46. Allemand D, TambuttE E, Girard JP, Jaubert J (1998) Organic matrix synthesis in the scleractinian coral *stylophora pistillata*: Role in biomineralization and potential target of the organotin tributyltin. *J Exp Biol* 201(pt 13):2001–2009.
47. Takeichi M (2007) The cadherin superfamily in neuronal connections and interactions. *Nat Rev Neurosci* 8(1):11–20.
48. Shoguchi E, et al. (2013) Draft assembly of the S*ymbiodinium minutum* nuclear genome reveals dinoflagellate gene structure. *Curr Biol* 23(15):1399–1408.
49. Bertucci A, et al. (2013) Carbonic anhydrases in anthozoan corals-a review. *Bioorg Med Chem* 21(6):1437–1450.
50. Leggat W, Badger MR, Yellowlees D (1999) Evidence for an inorganic carbon-concentrating mechanism in the symbiotic dinoflagellate *Symbiodinium* sp. *Plant Physiol* 121(4):1247–1256.
51. Cohen AL, McConnaughey TA (2003) Geochemical perspectives on coral mineralization. *Rev Mineral Geochemistry* 54:151–187.
52. Cuif J-P, Dauphin Y (1998) Microstructural and physico-chemical characterization of 'centers of calcification' in septa of some recent scleractinian corals. *Paläontologische Zeitschrift* 72(3-4):257–269.
53. Spudich JA (2011) Biochemistry. Molecular motors, beauty in complexity. *Science* 331(6021):1143–1144.
54. Asselman M, Verhulst A, De Broe ME, Verkoelen CF (2003) Calcium oxalate crystal adherence to hyaluronan-, osteopontin-, and CD44-expressing injured/regenerating tubular epithelial cells in rat kidneys. *J Am Soc Nephrol* 14(12):3155–3166.
55. Mann S (1983) Mineralization in biological systems. *Structure and Bonding* 54: 125–174.
56. Barnes DJ, Crossland CJ (1980) Diurnal and seasonal variations in the growth of a staghorn coral measured by time-lapse photography. *Limnol Oceanogr* 25(6): 1113–1117.
57. Gladfelter EH (1983) Skeletal development in *Acropora cervicornis*. II. Diel patterns of calcium carbonate accretion. *Coral Reefs* 2:91–100.
58. Vago R, Gill E, Collingwood JC (1997) Laser measurements of coral growth. *Nature* 386(6620):30–31.
59. Domart-Coulon I, et al. (2014) Simultaneous extension of both basic microstructural components in scleractinian coral skeleton during night and daytime, visualized by in situ ^{86}Sr pulse labeling. *J Struct Biol* 185(1):79–88.
60. Drake JL, Mass T, Falkowski PG (2014) The evolution and future of carbonate precipitation in marine invertebrates: Witnessing extinction or documenting resilience in the Anthropocene? *Elementa. Science of the Anthropocene* 2(1):000026.
61. Park H, Mcginn PJ, Morel FMM (2008) *Expression of Cadmium Carbonic Anhydrase of Diatoms in Seawater* (Inter-Research, Oldendorf/Luhe, Germany).

Downloaded at Palestinian Territory, occupied on December 9, 2021

www.manaraa.com